A comparison of the bond behavior of PBO-FRCM composites determined by double-lap and single-lap shear tests

L.H. Sneed [a, *], T. D'Antino [b], C. Carloni [c], C. Pellegrino [d]

[a] Missouri University of Science and Technology, 1401 North Pine Street, Rolla, MO 65409, USA
[b] University of Patras, Rio Achaia, Patras, Greece
[c] University of Bologna, Viale Risorgimento 2, 40136 Bologna, Italy
[d] University of Padova, Via Marzolo 9, 35131 Padova, Italy

Received 25 October 2014 Received in revised form
3 April 2015
Accepted 28 July 2015
Available online 5 September 2015

1. Introduction

Fiber-reinforced composite materials are widely used for strengthening, repairing, and rehabilitation of reinforced concrete (RC) structural members, offering sustainable alternatives to new construction. The use of externally-bonded composite systems for these purposes is attractive since they are easy to install, have high strength-to-weight ratio, and have suitable mechanical properties. The bond behavior of externally-bonded fiber-reinforced polymer (FRP) composite systems, comprised of continuous fibers (usually carbon, glass, or aramid) and an organic matrix (typically epoxy), has been studied extensively over the past several decades [1–6]. As the knowledge of FRP composite strengthening systems has become more advanced and their use more common, alternative types of composites are being explored for different applications. Recently a new type of binder called "*inorganic matrices*" has been developed and shown interesting potential as a replacement for organic matrices in composites [7]. Inorganic matrices are cement-based mortars comprised of ordinary cement with the addition of silica fume, nanoparticles, and/or polymers that increase the strength and bond characteristics. Composite materials that employ cement-based mortars are usually referred to as fiber-reinforced cementitious matrix (FRCM) composites [8]. The use of inorganic matrices in fiber-reinforced composites can overcome some of the limitations related to the use of organic matrices in FRP composites, such as degradation due to UV exposure, poor performance at temperatures close to or above the matrix glass transition temperature, and lack of compatibility with the substrate [7,8].

The FRCM-concrete interface has recently been studied using single-lap [9–12] or double-lap [13,14] direct shear tests. Results have shown that debonding of the FRCM-concrete interface occurs within the composite itself at the fiber–matrix interface, as opposed to the composite–concrete interface with FRP [1]. Furthermore, interlocking among the fibers, and between the fibers and matrix, has been shown to influence the load response of FRCM composites in single-lap shear tests [10,11]. However, the load response determined from the two test types has not yet been compared.

* Corresponding author. Missouri University of Science and Technology, 1401 North Pine Street, Rolla, MO, 65409, USA.
E-mail addresses: sneedlh@mst.edu (L.H. Sneed), dantino@upatras.gr (T. D'Antino), christian.carloni@unibo.it (C. Carloni), carlo.pellegrino@unipd.it (C. Pellegrino).

This paper examines the results of an experimental investigation conducted to study the bond behavior and stress-transfer mechanism of FRCM composites externally bonded to a concrete substrate using two different types of direct shear tests. The FRCM composite investigated in this study is comprised of a polyparaphenylene benzobisoxazole (PBO) fiber net and polymer modified cement-based matrix. Results of 16 double-lap shear tests with different bonded lengths and widths of the composite strips are presented and discussed. Findings are compared with those from 58 single-lap shear tests of the same composite previously reported by the authors [10] to examine the influence of the different direct shear test types on the bond behavior of the FRCM composites applied to concrete supports.

2. Materials and methods

2.1. Materials

The FRCM composite material consisted of a PBO fiber net and a cementitious matrix. The PBO fiber net was made of bidirectional rovings spaced at 10 and 20 mm (0.4 and 0.8 in.) on center in the two orthogonal directions. The total weight of fibers in the net was 88.0 g/m^2 (0.00013 lb/in.^{2}), with 70.2 g/m^2 (0.00010 lb/in.^{2}) and 17.8 g/m^2 (0.000025 lb/in.^{2}) in the longitudinal and transversal directions, respectively. The nominal width b^* and average thickness t^* of one fiber bundle were 5 mm (0.2 in.) and 0.092 mm (0.0036 in.), respectively. It should be noted that the definition of average thickness t^* in this paper is different from the equivalent thickness of the fabric given by the manufacturer [15], and therefore the values are different. The equivalent thickness provided by the manufacturer is obtained by assuming the fibers are spread evenly over the entire width of the composite rather than bundled. In this paper t^* represents the thickness of a single fiber bundle, which is assumed to have a rectangular cross section of width b^*. All transversal bundles of the fiber net were on one side of the longi-tudinal bundles. Tensile strength, ultimate strain, and elastic modulus of the fibers measured by the authors were 3014 MPa (440 ksi), 0.0145, and 206 GPa (29,900 ksi), respectively. Additional information on the fiber tensile tests is reported in Refs. [9–11]. The matrix was comprised of "high-fineness cement, an adhesion promoter, inorganic nanoparticles, microaggregates, and a polycarboxylate water-reducing admixture. This matrix was designed to achieve chemical bond with the PBO fibers" [8]. The average compressive strength and splitting tensile strength of the matrix was measured using at least two 50 × 100 mm (2 × 4 in.) cylinders cast from each batch of mortar used to cast the composites and were 28.4 MPa (4050 psi) (CoV = 0.092) and 3.5 MPa (520 psi) (CoV = 0.231), respectively.

The concrete prisms were constructed with normalweight concrete with portland cement (Type 1) without admixtures. The prisms were cast from the same concrete batch used to cast the 510 mm (20 in.) long blocks of the single-lap shear tests reported by the authors in Ref. [10]. The maximum aggregate size was 9.5 mm (0.375 in.). The average compressive strength and splitting tensile strength of concrete measured using six 100 × 200 mm (4 × 8 in.) cylinders cast from the same batch of concrete used to cast the prisms were 33.5 MPa (4860 psi) (CoV = 0.085) and 3.0 MPa (420 psi) (CoV = 0.042), respectively.

2.2. Methods

Sixteen specimens presented in this paper were tested using the double-lap (direct) shear test to study the bond behavior of PBO-FRCM composites bonded to a concrete substrate. Two FRCM composite strips were bonded to the surface of two concrete blocks (prisms). Each composite strip had two bonded regions of the same length, one on each of the two prisms (Fig. 1). The concrete prisms were 125 mm wide × 125 mm deep × 375 mm long (5 in. × 5 in. × 15 in.). The concrete prisms were sandblasted prior to applying the composite strips on opposite faces. Only the formed faces of the prisms were used to bond the composite strips; the face of each prism that was troweled smooth after casting and its opposite face were disregarded. The matrix was applied from the edge of the external longitudinal bundle on one side of the fiber strip to the edge of the external longitudinal bundle on the other side of the fiber strip along the length of the strip. A 4 mm (0.15 in.) thick layer of matrix (internal layer) was applied to the concrete using molds to control the composite width and thickness. A single layer of PBO fiber net was applied onto the internal matrix layer, and the fibers were pressed delicately onto the matrix to maintain their alignment and assure proper impregnation by the matrix. The fiber strip was positioned such that it extended slightly beyond the end of the matrix at the free ends of the composite strip as shown in Fig. 2a. A second (external) 4 mm thick layer of matrix was applied over the PBO fiber net. The thickness of the matrix layers was in accordance with the manufacturer's recommendations [15]. The fiber strip was oriented such that the transversal fiber bundles were placed against the external layer of matrix for all specimens. The bonded width b_1 and bonded length ℓ of the composite were varied. Table 1 lists the double-lap shear test specimens presented. Spec-imens were named following the notation DDS_X_Y_Z, where DDS indicates that the specimen was tested in double-lap direct shear, X = bonded length (ℓ) in mm, Y = bonded width (b_1) in mm, and Z = specimen number.

Force F was applied to each prism by a steel T-frame comprised of a steel rod with a steel plate welded to one end, and the concrete prisms were pulled apart (Fig. 1). The rod was placed through an embedded sleeve aligned with the longitudinal axis of the prism and was clamped to the testing machine at the loaded end. The inside diameter of the sleeve was slightly larger than that of the rod. Tests were conducted under displacement control using a close-loop servo-hydraulic universal testing machine. The average of four linear variable displacement transducers (LVDTs), two of which were attached to the concrete surface adjacent to the composite strip on each face of the lower prism and aligned with the beginning of the bonded region, was increased at a constant rate of 0.00084 mm/s (0.000033 in./s) for all tests. The LVDTs reacted off of thin aluminum L-shaped bent plates that were attached to the surface of the upper concrete prism as shown in Figs. 1 and 2a and positioned near the beginning of the composite region. The positions of the L-shaped plates needed to be adjusted for each specimen in order to accommodate the working range of the LVDTs. Data were recorded by a data acquisition system at a rate of 10 measurements per second. The length of the unbonded region of the composite $\ell_{unbonded}$ (shown in Fig. 1) at the start of the test was 100 mm (4 in.), which included an initial gap between the two prisms of 25 mm (1 in.) corresponding to the thickness of the two plates at the ends of the steel T-frames (Fig. 1).

3. Experimental results

Failure of all double-lap shear specimens was debonding of one composite strip, where debonding was characterized by slippage between the fibers and matrix within the composite strip. As the displacement (average of the four LVDT readings, LVDTavg) was gradually increased, cracks formed in the matrix of the composite strips within the unbonded region as shown in Fig. 2b. These cracks opened with increasing displacement. Increased displacement resulted in increased force until the peak (ultimate) force was reached. After the peak force was reached, lateral translation of the

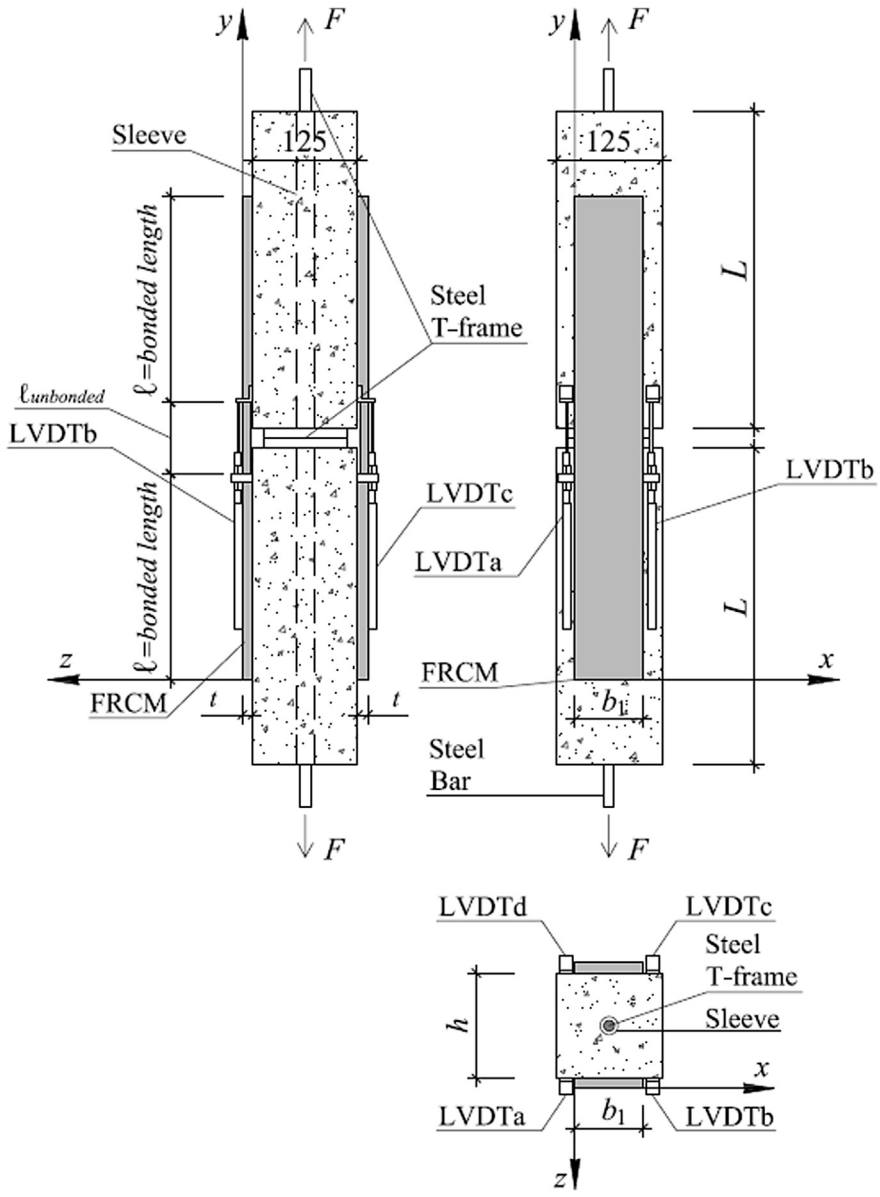

Fig. 1. Double-lap shear test setup.

ends of the two concrete prisms occurred in the z-direction in Fig. 1 causing rotation of the prisms relative to their initial vertical alignment, which was visibly apparent from the side of the specimen as shown in Fig. 2c. This visual observation was also confirmed by differences in the displacement measured by the four individual LVDTs, the average of which was used to control the displacement rate. Lateral translation was caused by unsymmetrical debonding of the composite strips. Slippage between the longitudinal fibers and matrix could be observed visually after the peak force was reached as the free end of the fiber strip advanced into the matrix. However, no measurement of the free end slip was considered in this study. No damage was observed to the concrete prisms. The peak force F^* applied to each double-lap shear test specimen is reported in Table 1.

Fig. 3 illustrates the measured response of representative double-lap shear test specimens. Fig. 3a and b plot the total force F applied to the test specimen versus individual displacement measurements from LVDTa, LVDTb, LVDTc, and LVDTd recorded during testing of specimens DDS_330_34_1 and DDS_330_80_1, respectively. The LVDT names are defined in Fig. 1. LVDTavg is also plotted in the graphs. After the peak force was reached, Fig. 3a and b show that the displacement measured on the opposite faces of the prisms eventually progressed in opposite directions, which indicates that the prisms rotated relative to their initial vertical alignment (see Fig. 2c). This post-peak response was characteristic of all double-lap shear tests conducted in this study and was caused by the unsymmetrical debonding of the composite strips (i.e., simultaneous debonding of both strips did not occur). Finally, Fig. 3a and b show a near-constant load region at the end of the test associated with increasing displacement of the LDVTs on the side of the prism where debonding initially occurred (LVDTa and LVDTb for specimens DDS_330_34_1 and DDS_330_80_1). On the opposite side of the prism, the displacement measured by the LDVTs (LVDTc and LVDTd for specimens DDS_330_34_1 and DDS_330_80_1) remained nearly constant, which indicates a continually changing center of rotation of the test specimen. For specimen

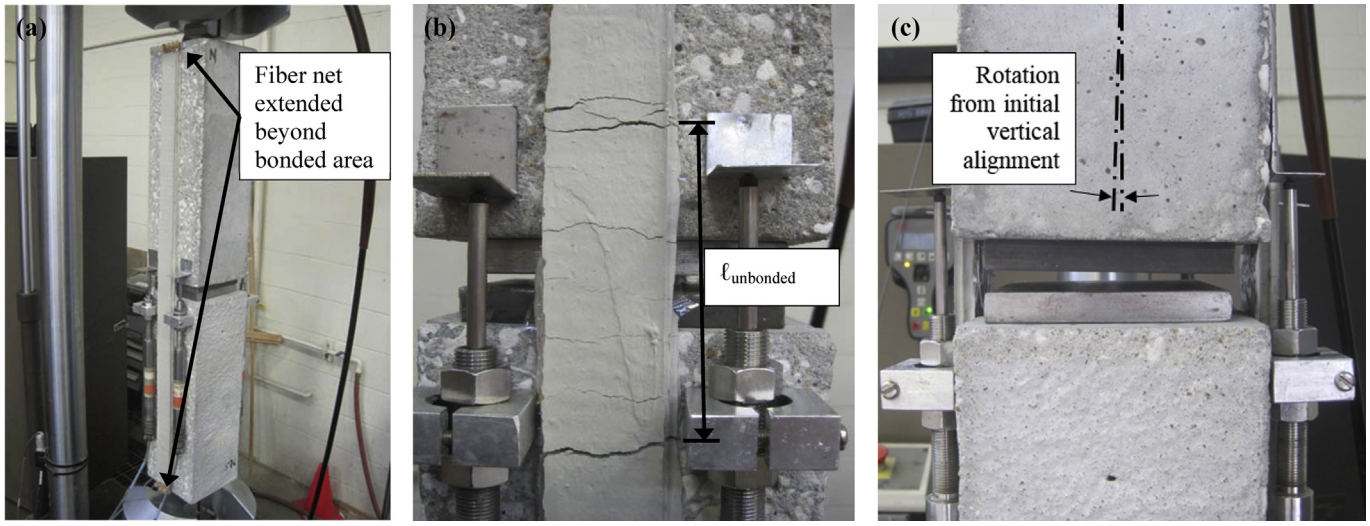

Fig. 2. a) Photo of test setup b) Cracks in matrix of unbonded region c) Rotation of the two concrete blocks relative to initial alignment after peak load (specimen DDS_330_34_1 shown).

DDS_330_34_1, Fig. 3a shows that the displacement measured by the pairs of LVDTs on the opposite faces of the prism corresponding to the two composite strips was consistent throughout the test, which indicates that the two prisms did not rotate in the plane of the composite strips (about the z-axis in Fig. 1) significantly during the test. Fig. 3b indicates that a slight amount of rotation in the plane of the composites occurred during testing of specimen DDS_330_80_1 before and after the peak force was reached. Of the 16 double-lap shear specimens tested, seven showed a response similar to that shown in Fig. 3a, and nine showed a response similar to that shown in Fig. 3b.

Fig. 3c and d plot the displacement measured by each LVDT throughout the test (plotted as virtual time) and the average of the four LVDTs used to control the loading rate for specimens DDS_330_34_1 and DDS_330_80_1, respectively. Fig. 3c and d shows that after the peak force was reached (indicated in the figures), the rate of displacement measured by the LVDTs on the opposite faces of the prisms changed and eventually decreased with increasing virtual time on the side of the prism where debonding did not initially occur. For specimen DDS_330_80_1, the displacement measured by LVDTc and LVDTd started to decrease immediately after the peak load was reached (Fig. 3d). This result suggests that debonding likely occurred in only one of the composite strips, as discussed further in Section 4.2. For specimen DDS_330_34_1, displacement measured by LVDTc and LVDTd started to decrease at a displacement larger than the displacement corresponding to the peak force (Fig. 3c). This result suggests that debonding may have occurred to some degree in both composite strips (Section 4.2), although this hypothesis cannot be confirmed without additional measurements.

If perfect symmetry is assumed, the applied load P in each of the two bonded composites can be related to the total force F applied to the test specimen by Eq. (1):

$$P = \frac{F}{2} \tag{1}$$

The peak load P^* in the composite strip computed using Eq. (1) corresponding to the maximum force F^* is reported for each specimen in Table 1.

Table 1
Double-lap shear test specimens.

Specimen	F^*		$P^* = F^*/2$		σ^*		$P_{II}{}^*$		$\sigma_{II}{}^*$	
	kN	(kip)	kN	(kip)	MPa	(ksi)	kN	(kip)	MPa	(ksi)
DDS_100_60_1	8.44	(1.90)	4.22	(0.95)	1310	(190)	4.17	(0.94)	1295	(188)
DDS_100_60_2	8.49	(1.91)	4.25	(0.95)	1319	(191)	4.22	(0.95)	1311	(190)
DDS_200_60_1	11.32	(2.54)	5.66	(1.27)	1757	(255)	5.65	(1.27)	1755	(254)
DDS_200_60_2	10.45	(2.35)	5.22	(1.17)	1622	(235)	5.18	(1.16)	1609	(233)
DDS_250_60_1	11.24	(2.53)	5.62	(1.26)	1746	(253)	5.55	(1.25)	1724	(250)
DDS_250_60_2	12.17	(2.74)	6.09	(1.37)	1890	(274)	6.10	(1.37)	1894	(275)
DDS_330_34_1	6.83	(1.53)	3.41	(0.77)	1855	(269)	3.41	(0.77)	1853	(269)
DDS_330_34_2	6.63	(1.49)	3.31	(0.75)	1801	(261)	3.31	(0.74)	1799	(261)
DDS_330_60_1	11.10	(2.49)	5.55	(1.25)	1723	(250)	5.33	(1.20)	1655	(240)
DDS_330_60_2	12.15	(2.73)	6.08	(1.37)	1887	(274)	6.00	(1.35)	1863	(270)
DDS_330_60_3	11.74	(2.64)	5.87	(1.32)	1823	(264)	5.88	(1.32)	1826	(265)
DDS_330_80_1	15.76	(3.54)	7.88	(1.77)	1903	(276)	7.68	(1.73)	1855	(269)
DDS_330_80_2	16.46	(3.70)	8.23	(1.85)	1987	(288)	8.03	(1.81)	1940	(281)
DDS_330_80_3	14.61	(3.28)	7.31	(1.64)	1765	(256)	7.28	(1.64)	1758	(255)
DDS_330_100_1	21.21	(4.77)	10.60	(2.38)	2095	(304)	10.62	(2.39)	2099	(304)
DDS_330_100_2	20.82	(4.68)	10.41	(2.34)	2057	(298)	10.31	(2.32)	2038	(296)

Note 1: DDS_X_Y_Z where DDS = double-lap direct shear specimen, X = bonded length (ℓ) in mm, Y = bonded width (b_1) in mm, and Z = specimen number.

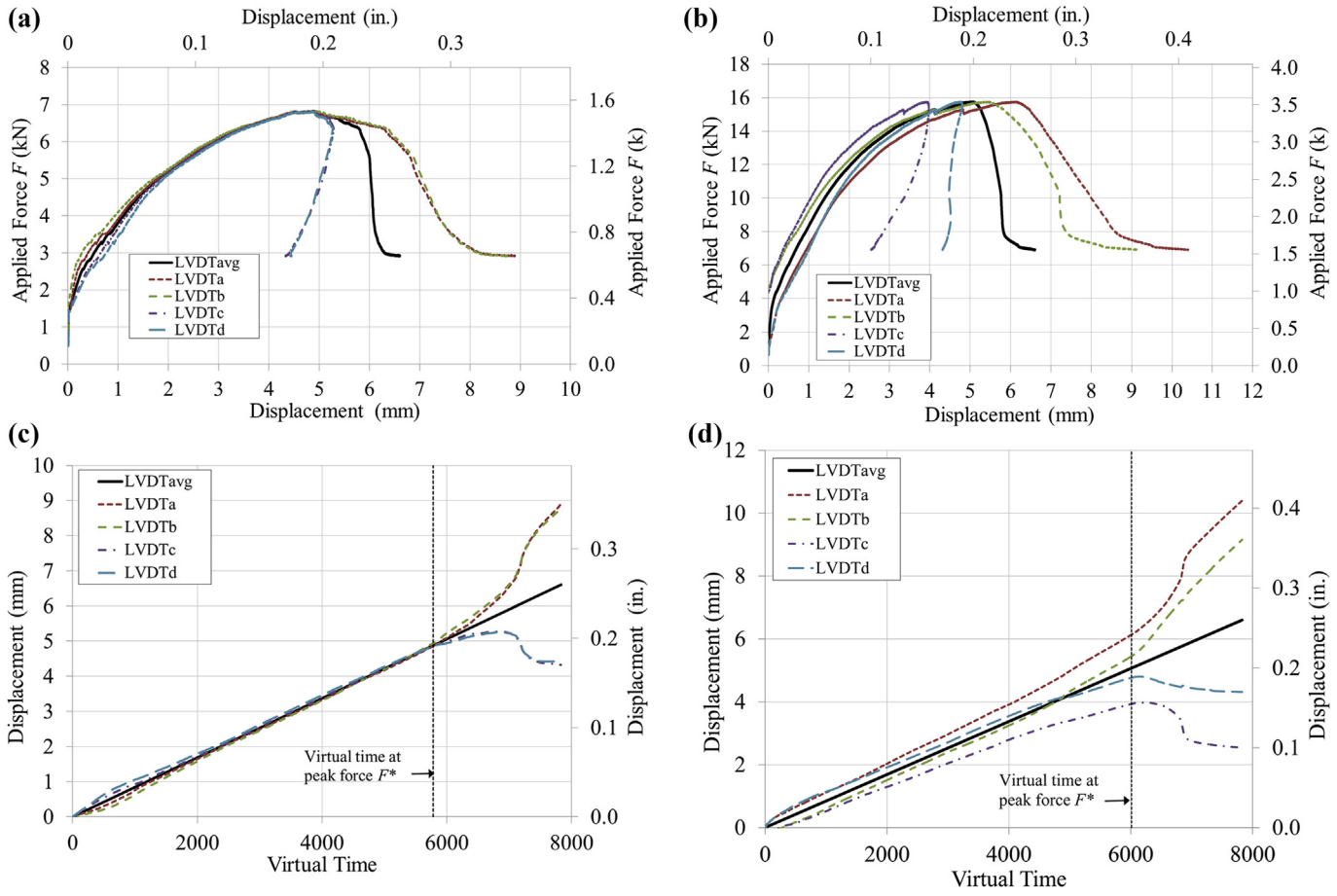

Fig. 3. a) Applied force *F* vs. LVDT measurements for specimen DDS_330_34_1 b) Applied force *F* vs. LVDT measurements for specimen DDS_330_80_1 c) LVDT measurements for specimen DDS_330_34_1 d) LVDT measurements for specimen DDS_330_80_1.

The normal stress σ in the composite associated with the applied load *P* in the composite strip is defined by Eq. (2):

$$\sigma = \frac{P}{nb^*t^*} \tag{2}$$

where *n* is the number of longitudinal fiber bundles. The nominal area of the longitudinal fiber bundles nb^*t^* was used to compare specimens of different bonded widths [10–12]. The ultimate stress σ^* in the composite strip computed using Eq. (2) corre-sponding to the peak load P^* is reported for each specimen in Table 1.

Fig. 4 shows the relationship between the ultimate stress σ^* and composite bonded length ℓ for specimens with a composite width b_1 equal to 60 mm (2.4 in.), termed the DDS_XXX_60 series. Average values of σ^* for specimens in the DDS_XXX_60 series with the same bonded length are also plotted in the graph with solid markers. Additionally, results from double-lap shear tests of the same composite reported by D'Ambrisi et al. [14] are included in the graph for comparison. For the DDS_XXX_60 series, Fig. 4 shows that the ultimate stress increases with increasing bonded length at a decreasing rate. This trend is consistent with the double-lap shear test results from D'Ambrisi et al. [14].

Fig. 5 shows the relation between ultimate stress σ^* and com-posite bonded width b_1 for specimens in Table 1 with the same bonded length (ℓ = 330 mm [13 in.]), termed the DDS_330 series. Four different bonded widths are shown, namely 34 mm (1.3 in.), 60 mm (2.4 in.), 80 mm (3.1 in.), and 100 mm (3.9 in.). Average values of σ^* for specimens in the DDS_300 series with the same bonded width are also plotted in the graph with solid markers. Also, the average value of σ^* for all specimens in the DDS_330 series is reported in the figure. Unlike for the case of FRP composites [16], results from the double-lap shear tests suggest that a width effect does not exist for this type of composite.

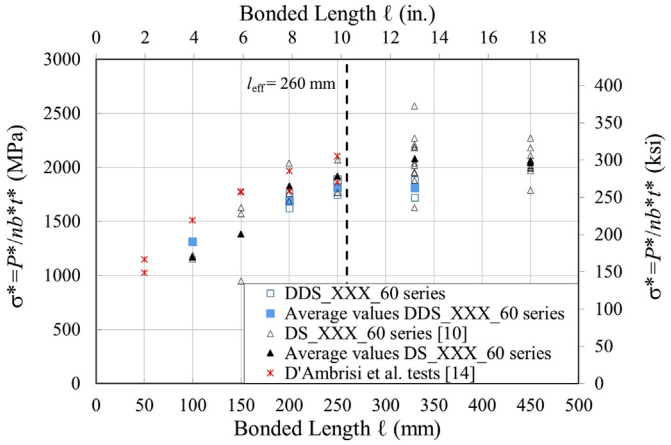

Fig. 4. Ultimate Stress σ^* vs. bonded length ℓ for DDS_XXX_60 series and DS_XXX_60 series.

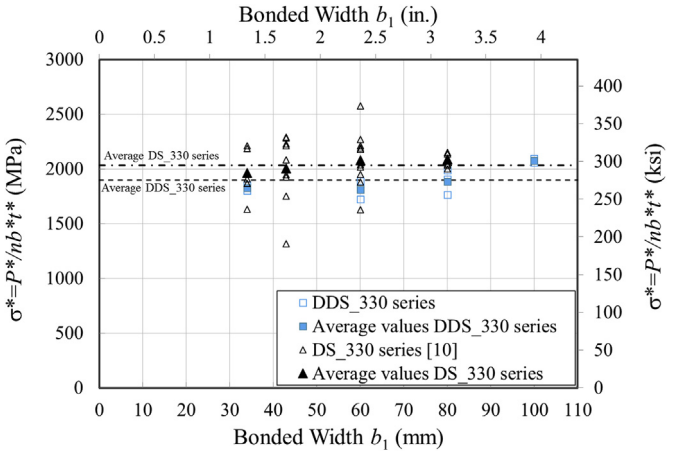

Fig. 5. Ultimate stress σ* vs. bonded width b_1 for DDS_330 series and DS_330 series.

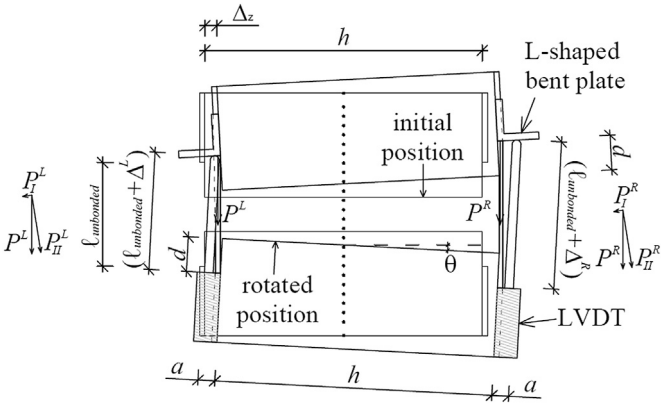

Fig. 6. Determination of applied loads P_{II}^L and P_{II}^R and global slips g^L and g^R from LVDT measurements.

4. Analysis and discussion

4.1. Determination of the applied load P_{II} − global slip g response

The bond between a composite and substrate is described in terms of the load applied to the composite versus slip at the loaded end of the composite. Since debonding of the PBO-FRCM composite occurs at the matrix−fiber interface, slip of the composite is the displacement of the fibers relative to the embedding matrix. The authors previously defined the term "global slip" as the displacement of the fibers relative to the embedding matrix at the start (loaded end) of the bonded length [10−12]. For the case of the double-lap shear tests, with two bonded composites, the graphs in Fig. 3 clearly identify different responses of the two PBO-FRCM composite strips, especially after the peak force is reached. Therefore, the applied load − global slip response of the bonded composite reported for a given double-lap shear test specimen should be the response of the composite strip that debonded first. However, it must be pointed out that the response of the composite strip that debonds initially is not independent of that of the composite strip on the opposite face because of load redistribution that occurs throughout the entire test. Load redis-tribution causes a marked difference in the response of the two composite strips after unsymmetrical debonding occurs (see Fig. 3), although it can also occur prior to debonding due to a slight eccentricity of the force applied to the test specimen and/or var-iations in the local bond characteristics of two composite strips [11,12].

The distribution of the total applied force F to the two composite strips was determined in this study from the displacements measured by the four LVDTs used to control the test. Simple geometrical relations were used to compute the angle of rotation θ about the x-axis (the x-axis is shown in Fig. 1) of the concrete prisms relative to their initial vertical alignment based on the differences in LVDT measurements as shown in Fig. 6. Angle θ was determined from Eq. (3):

$$\tan 2\theta = \frac{\Delta^R - \Delta^L}{h + 2a} \tag{3}$$

where h is the width of the block; a is the distance from the face of block to the center of the LVDT; Δ^L and Δ^R are the average displacements measured by the two LVDTs on the corresponding sides given by Eq. (4a) and (4b):

$$\Delta^L = \frac{LVDTa + LVDTb}{2}; \quad \Delta^R = \frac{LVDTc + LVDTd}{2} \tag{4a) and (4b)}$$

The horizontal translation Δ_z of the points on the block corresponding to the beginning of the bonded length is given by Eq. (5):

$$\Delta_z = \sin\theta(L - d) \tag{5}$$

where L is the length of the block (Fig. 1), and d is the distance from the end of the block to the start of the bonded length shown in Fig. 6.

The applied load P^L and P^R (in the direction of the applied force F) in each composite strip was computed using Eqs. (6) and (7), respectively:

$$P^L = F - P^R \tag{6}$$

$$P^R = \frac{F\left(\frac{h}{2} - \Delta_z\right)}{z} \tag{7}$$

where z is the horizontal projection of the block width h; $z = h\cos\theta$. Superscripts "L" and "R" are used to denote the composite strips on the left and right sides of the block, respectively. LVDTa and LVDTb were considered to be on the left side of the block, and LVDTc and LVDTd were on the right side.

The component of the applied load in the plane of the composite strips, P_{II}^L and P_{II}^R, was computed using Eqs. (8) and (9), respectively:

$$P_{II}^L = P^L \cos\theta \tag{8}$$

$$P_{II}^R = P^R \cos\theta \tag{9}$$

Subscript "II" is used to denote the Mode-II component of the applied load (parallel to the composite strip), as debonding is typically studied as a Mode-II fracture mechanics problem [1−3]. It should be noted that the out-of-plane force components of the applied load P^L and P^R, shown as P_I^L and P_I^R in Fig. 6, have directions resulting in friction for the composite strip that debonds first, and peeling (Mode-I) for the other composite strip.

Using Eqs. (10) and (11), the corresponding global slip g^L and g^R in each composite strip was determined from the LVDT measurements (considering angle θ) and by subtracting the elastic

elongation of the composite associated with the length of the unbonded region $\ell_{unbonded}$, which was determined from the applied load in the composite strip on the corresponding side:

$$g^L = \frac{1}{2}\left[\frac{\Delta^L}{\cos\theta} - \frac{P^L \ell_{unbonded}}{AE}\right] \quad (10)$$

$$g^R = \frac{1}{2}\left[\left(\frac{\cos 2\theta}{\cos\theta}\right)\Delta^R - \frac{P^R \ell_{unbonded}}{AE}\right] \quad (11)$$

where A is the cross-sectional area and E is the modulus of elasticity of the composite in the unbonded region (discussed in the next paragraphs). The effect of the out-of-plane displacement of the fi-bers relative to the embedding matrix slip was neglected in the calculation of global slip.

Using this procedure, the applied loads P_{II}^L and P_{II}^R and corresponding global slips g^L and g^R were computed for the entire load response of both composite strips for each specimen. It should be noted that several assumptions were adopted in this procedure: 1) the LVDTs are assumed to be aligned with the start of the bonded regions of the composite strips; 2) elastic elongation occurs uniformly along the unbonded length; 3) the top and bottom prisms rotate from their initial vertical alignment equally (angle θ is the same for both prisms); 4) the effects of block rotation in the plane of the composite strips are not considered (non-uniform load distri-bution within the plane of the composite strip is neglected); and 5) global slip occurs equally in both bonded regions of the same composite strip. The first assumption was necessary in the present study to estimate the elastic elongation of the composite in the unbonded region to enable the calculation procedure. This assumption will introduce slight errors into the values computed because of the position of the L-shaped aluminum plates in this study, as discussed in Section 2.2. The fifth assumption implies that debonding occurs simultaneously and equally in both bonded regions of the same composite strip, which may not always be the case and is difficult to confirm. This assumption is discussed further in Section 4.2.

As an example, Fig. 7a shows the $P_{II}^L - g^L$ and $P_{II}^R - g^R$ responses determined for specimen DDS_330_34_1, where the $P_{II}^L - g^L$ response is associated with the composite strip that debonded first as can be seen from the post-peak displacement response in Fig. 3a. In the pre-peak response region, the region of the curves plotted with a different linetype (short dash) represent the region in which the cross-sectional area A and modulus of elasticity E transition from the values associated with composite, $A_{composite}$ and $E_{composite}$, to those associated with the fibers, A_{fiber} and E_{fiber}. The transition region was assumed to start after first cracking of the matrix, where cracking was determined by the measured tensile strength of the matrix (Section 2.1), and end at a point that was arbitrarily assumed based on a reasonable load response. Since it was not possible to establish the sequence of cracking, this transition was assumed to be linear in the graph. The elastic modulus of the composite $E_{com\text{-}posite}$ was estimated using Eq. (12):

$$E_{composite} = E_{fiber}v_{fiber} + E_{matrix}v_{matrix} \quad (12)$$

where E_{fiber} is the measured elastic modulus of the fibers, v_{fiber} is the volume fraction of the fibers, E_{matrix} is the elastic modulus of the matrix reported by the manufacturer [15], and v_{matrix} is the volume fraction of the matrix.

Fig. 7b plots the values of the applied loads P_{II}^L and P_{II}^R and global slips g^L and g^R determined for specimen DDS_330_34_1 for the duration of the test (plotted as virtual time). Additionally, rotation angle θ is plotted in the graph. In the plots of global slips g^L and g^R, the region of the curve plotted with a different linetype (short dash) represents the region in which area A transitions from $A_{composite}$ to A_{fiber} and E transitions from $E_{composite}$ to E_{fiber} after first cracking of the matrix, as discussed in the previous paragraph. Fig. 7b shows that applied loads P_{II}^L and P_{II}^R are consistent until the peak load is reached. Immediately after the peak load is reached, the global slip continues to increase in both composite strips with a slight reduction in applied load. The applied load starts to decrease because the bond mechanism is no longer fully established for the composite strip that initially debonded. The fact that the global slip continues to increase in the other composite strip suggests that debonding may have initiated in that strip as well, although additional measurements are required to confirm this hypothesis. After the peak load (the virtual time at the measured peak force applied to the test specimen is indicated in Fig. 7b), the value of P_{II}^R is slightly larger than that of P_{II}^L due to increasing rotation (magnitude of angle θ) as a result of differences in global slips g^L and g^R in the two composite strips.

In the remaining figures in this paper, the $P_{II} - g$ relations presented for the double-lap shear specimens are those associated with the composite strip that initially debonded (e.g., $P_{II}^L - g^L$ for specimen DDS_330_34_1, see Fig. 7). The response of the other composite strip is not shown.

$P_{II} - g$ responses of representative specimens with different bonded lengths and the same bonded width in the DDS_XXX_60 series ($b_1 = 60$ mm [2.4 in.]) are plotted in Fig. 8. The $P_{II} - g$ relations

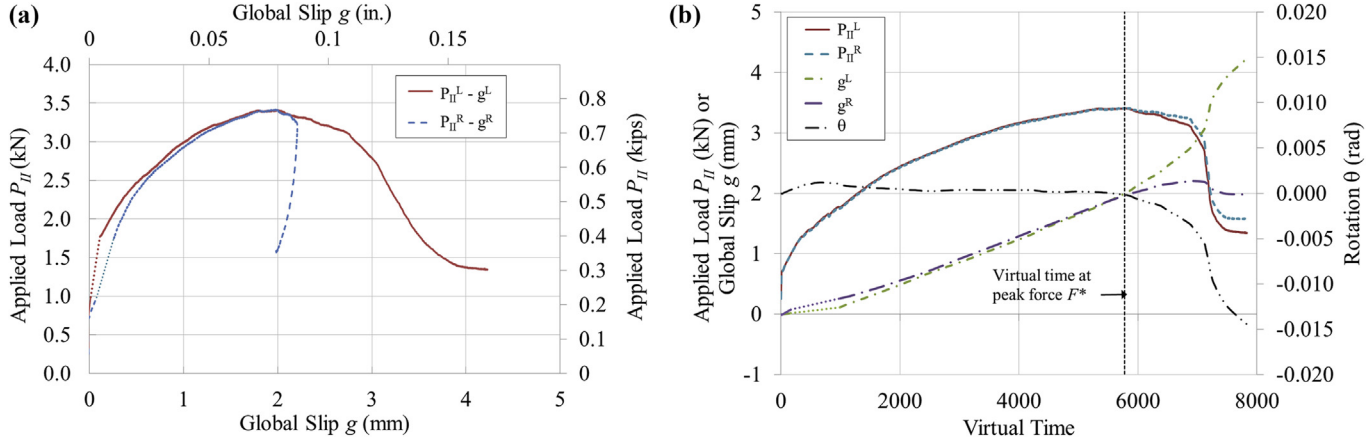

Fig. 7. a) $P_{II}^L - g^L$ and $P_{II}^R - g^R$ for specimen DDS_330_34_1 b) P_{II}^L, P_{II}^R, g^L, g^R, and θ versus virtual time for Specimen DDS_330_34_1.

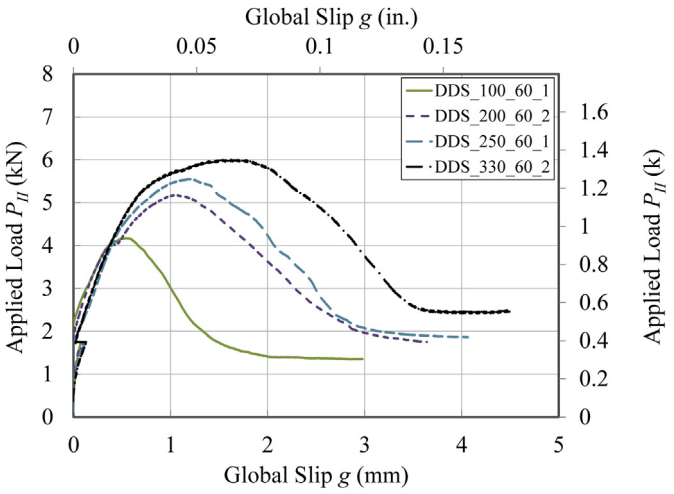

Fig. 8. Applied load P_{II} – global slip g responses for representative specimens (DDS_XXX_60 series).

shown are characteristic of the double-lap shear test specimens presented in this paper. Fig. 8 shows initial overlap in the linear pre-peak responses, and specimens with longer bonded lengths continuing up to higher peak load levels. The discontinuity in the initial portion of the responses is due to the abrupt change in A and E, which, in this graph, were assumed to change abruptly from $A_{composite}$ to A_{fiber} and $E_{composite}$ to E_{fiber} after initial cracking of the matrix, where cracking was determined by the measured tensile strength of the matrix.

$P_{II} - g$ responses of representative specimens of different composite bonded widths and the same bonded length in the DDS_330 series ($\ell = 330$ mm [13 in.]) are shown in Fig. 9a. Fig. 9b shows the responses of the same specimens in terms of normal stress σ_{II} defined using Eq. (2), with $\sigma = \sigma_{II}$ and $P = P_{II}$. Fig. 9a and b shows that in general, an initial linear response is followed by a non-linear response up to the peak (ultimate) load. The descending post-peak response has a variable gradient until a near-constant load region is reached.

The ultimate load P_{II}^* and the ultimate stress σ_{II}^* of each double-lap shear test specimen are summarized in Table 1, where P_{II}^* is determined using the procedure described in this section, and σ_{II}^* is computed by Eq. (2) with $P = P_{II}^*$. The difference between values of P^* approximated using Eq. (1) (i.e., assuming perfect symmetry) and P_{II}^* computed using the procedure in this section ranged from 0 to 4% for the double-lap shear tests presented in this paper, with an average percent difference of 1%. In general, good agreement is observed between the approximated values and the values determined using the procedure developed, which suggests that the use of Eq. (1) is reasonable for determining the applied load in each FRCM composite strip at the peak load. However, it is noted that this approximation cannot be used to describe the entire load-slip response of the composite, especially after debonding of one of the two composites strips occurs (see Fig. 7).

4.2. Comparison of double-lap and single-lap shear test results

This section compares the results of the double-lap shear tests presented in this paper with results of 58 single-lap shear tests of the same PBO-FRCM composite previously reported by the authors [10]. Single-lap shear tests selected for the comparison from Ref. [10] had a composite bonded width $b_1 = 60$ mm [2.4 in.], a composite bonded length $\ell = 330$ mm [13 in.], or both. The single-lap shear specimens selected and their peak load P^* and peak stress σ^* results are summarized in Table 2. Test specimen nomenclature is defined in a note at the bottom of the table. Results of the single-lap shear tests are included in Figs. 4, 5, and 9 to support the comparison with the double-lap shear tests. It should be noted that for the single-lap shear tests, the subscript "II" was not used in the applied load or normal stress variables in the reference [10] because the load was initially applied in the plane of the composite, and the out-of-plane component was neglected [17].

Fig. 9, which illustrates load responses of specimens with a composite bonded length $\ell = 330$ mm [13 in.] and different bonded widths, includes representative specimens from the DDS_330 series and single-lap shear specimen DS_330_60_D_3 for comparison. The load response of specimen DS_330_60_D_3 is representative of the single-lap shear specimens tested by the authors [10]. Fig. 9a and b shows that the shapes of the load responses of the double-lap shear specimens are similar to that of single-lap shear specimen with a few key differences. Fig. 9b shows that the global slip of the double-lap shear specimens is less than that of the single-lap shear specimen for a given load level. It should be noted that the global slip of the double-lap shear specimens is influenced by the calculation procedure employed in Section 4.1, including estimation of the elastic elongation of the composite in the unbonded region and the assumption that global slip occurs equally in both bonded regions of the same composite strip (assumption 5 in Section 4.1). If

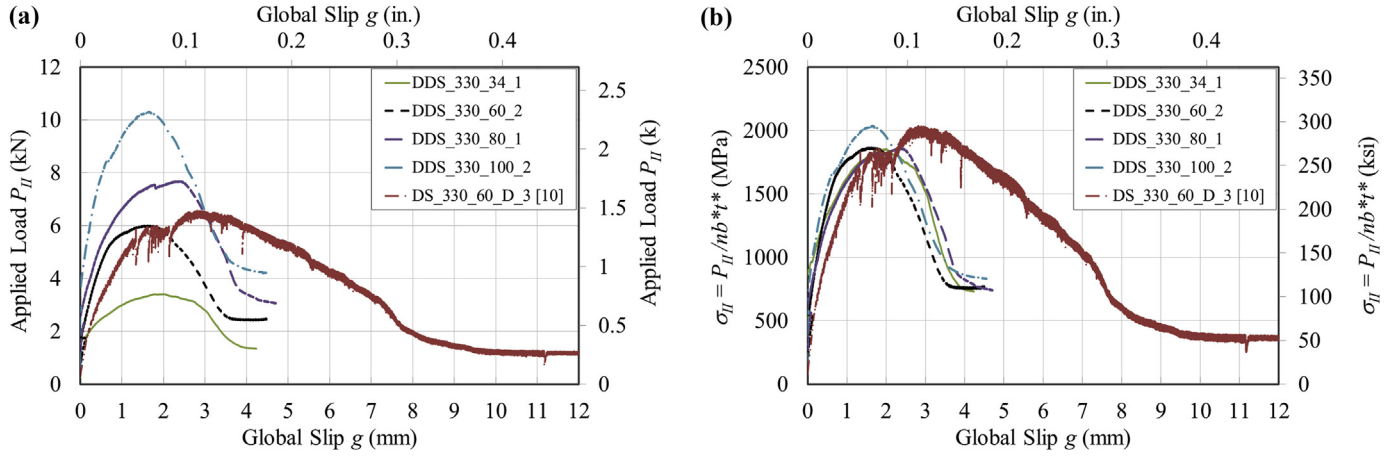

Fig. 9. a) Applied load P_{II} – global slip g responses for representative DDS_330_XX specimens. b) Normal stress σ_{II} vs. global slip g for representative DDS_330_XX specimens.

Table 2
Single-lap shear test specimens.

Specimen	P^*		σ^*		Specimen	P^*		σ^*	
	kN	(kip)	MPa	(ksi)		kN	(kip)	MPa	(ksi)
DS_100_60_1	3.69	(0.83)	1150	(167)	DS_330_60_4^T	6.50	(1.46)	2020	(293)
DS_100_60_2	3.83	(0.86)	1190	(173)	DS_330_60_5^T	6.28	(1.41)	1950	(283)
DS_100_60_3	3.77	(0.85)	1170	(170)	DS_330_60_6	7.01	(1.58)	2180	(316)
DS_150_60_1	5.25	(1.18)	1630	(236)	DS_330_60_D_1	8.29	(1.86)	2570	(373)
DS_150_60_2	5.04	(1.13)	1570	(228)	DS_330_60_D_2	7.12	(1.60)	2210	(321)
DS_150_60_3	3.05	(0.69)	950	(138)	DS_330_60_D_3	6.56	(1.47)	2040	(296)
DS_200_60_2	5.66	(1.27)	1760	(255)	DS_330_60_D_4	5.24	(1.18)	1630	(236)
DS_200_60_3	5.44	(1.22)	1690	(245)	DS_330_60_D_5	6.69	(1.50)	2080	(302)
DS_200_60_4	6.58	(1.48)	2040	(296)	DS_330_60_S_1	6.30	(1.42)	1960	(284)
DS_250_60_1	6.68	(1.50)	2070	(300)	DS_330_60_S_2	7.31	(1.64)	2270	(329)
DS_250_60_2	6.17	(1.39)	1920	(278)	DS_330_80_1	8.47	(1.90)	2050	(297)
DS_250_60_3	5.70	(1.28)	1770	(257)	DS_330_80_2	8.84	(1.99)	2140	(310)
DS_330_34_1^T	3.00	(0.67)	1630	(236)	DS_330_80_3	8.28	(1.86)	2000	(290)
DS_330_34_2^T	3.51	(0.79)	1910	(277)	DS_330_80_D_1	8.9	(2.00)	2150	(312)
DS_330_34_7	4.07	(0.91)	2210	(321)	DS_330_80_D_2	8.68	(1.95)	2100	(305)
DS_330_34_8	4.02	(0.90)	2180	(316)	DS_330_80_D_3	8.90	(2.00)	2150	(312)
DS_330_34_9	3.44	(0.77)	1870	(271)	DS_330_80_D_4	8.42	(1.89)	2030	(294)
DS_330_43_1^T	4.43	(1.00)	1930	(280)	DS_330_80_D_5	8.58	(1.93)	2070	(300)
DS_330_43_2^T	5.25	(1.18)	2280	(331)	DS_450_60_1	6.40	(1.44)	1990	(289)
DS_330_43_3	5.27	(1.18)	2290	(332)	DS_450_60_2	6.34	(1.43)	1970	(286)
DS_330_43_5	4.79	(1.08)	2080	(302)	DS_450_60_3	6.44	(1.45)	2000	(290)
DS_330_43_6	5.09	(1.14)	2210	(321)	DS_450_60_4	5.77	(1.30)	1790	(260)
DS_330_43_S_1^T	4.48	(1.01)	1950	(283)	DS_450_60_5	6.51	(1.46)	2020	(293)
DS_330_43_S_2^T	5.12	(1.15)	2230	(323)	DS_450_60_6	6.79	(1.53)	2110	(306)
DS_330_43_S_3^T	3.03	(0.68)	1320	(191)	DS_450_60_7	6.65	(1.49)	2070	(300)
DS_330_43_S_5	4.03	(0.91)	1750	(254)	DS_450_60_D_1	7.01	(1.58)	2180	(316)
DS_330_60_1^T	7.05	(1.58)	2190	(318)	DS_450_60_D_2	6.67	(1.50)	2070	(300)
DS_330_60_2^T	6.56	(1.47)	2040	(296)	DS_450_60_D_3	7.33	(1.65)	2280	(331)
DS_330_60_3^T	6.06	(1.36)	1880	(273)	DS_450_60_S_1	6.63	(1.49)	2060	(299)

Note 1: DS_X_Y_(S or D)_Z$^{(T)}$ where DS = single-lap direct shear specimen, X = bonded length (ℓ) in mm, Y = bonded width (b_1) in mm, S = presence of strain gauges mounted on the fiber net, D = specimen tested until a constant load at the end of the test was measured, Z = specimen number, and superscript T = fiber net oriented with the transversal fiber bundles directly against the matrix internal layer.

the global slip of the two bonded regions is indeed unequal, the computed values of global slip are underestimated, which may explain the difference in magnitude of global slip in the double-lap and single-lap shear tests. Fig. 9b also shows that the magnitude of the normal stress at the near-constant load region at the end of the test is larger for the double-lap shear tests than for the single-lap shear test.

Based on experimental and analytical evidence from the single-lap shear tests of the PBO-FRCM composite, the authors previously developed an idealized applied load-global slip response shown in Fig. 10a [10], which is briefly summarized herein. The first part of the idealized response is represented by a linear branch associated with elastic behavior of the bond between the fibers and the matrix (region O-A in Fig. 10a). Following, the response starts to be nonlinear; the interface between the fibers and the matrix experiences some micro-damage, and the value of the applied load P

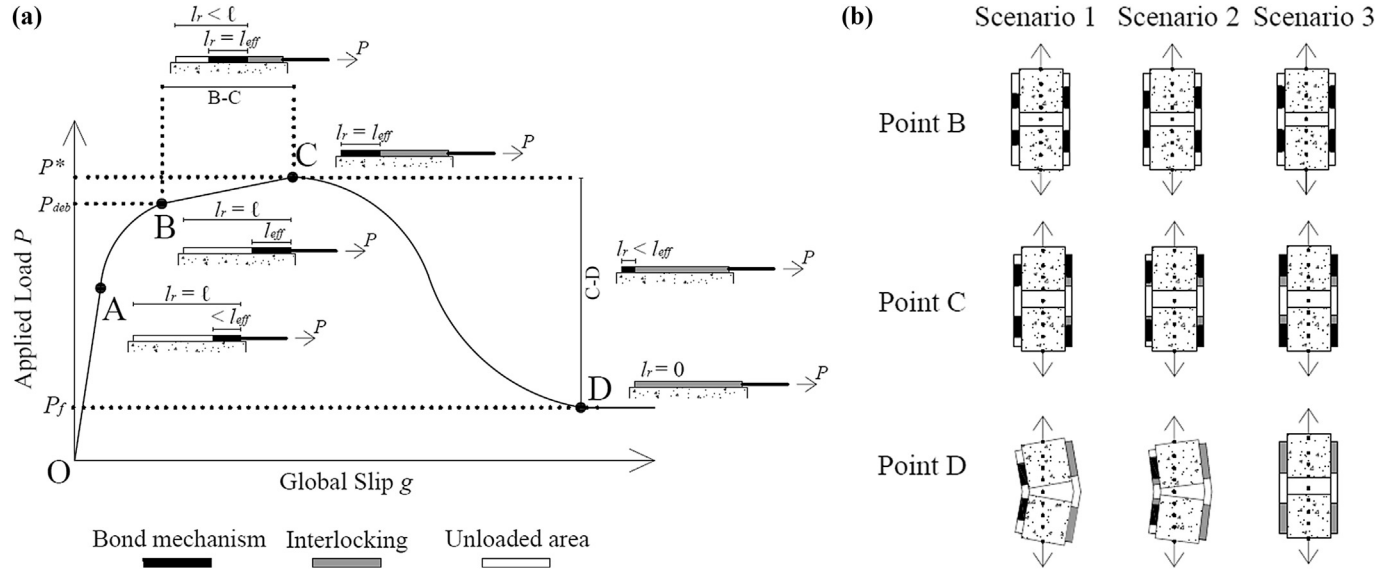

Fig. 10. a) Idealized applied load P – global slip g response determined from single-lap shear tests, b) Illustration of debonding scenarios of double-lap shear tests at key points of the idealized load response in (a).

increases until the onset of debonding at the matrix−fiber interface (point B). If the composite bonded length ℓ is equal to or longer than the effective bond length l_{eff}, defined as the minimum length needed to develop the load-carrying capacity of the interface [10−12], the stress transfer zone (STZ) [18] is fully established, and the applied load P at point B is equal to the debonding load P_{deb}. Once the debonding load is reached, interlocking between single fiber filaments and between fibers and matrix [19,20] occurs in the portion of the composite where the fibers have debonded. Consequently, an increase in the applied load P after debonding initiates is observed as the STZ translates along the bonded length towards the free end of the composite. Once the STZ reaches the free end of the composite, the maximum load P^* is reached (point C). (For the case of $\ell < l_{eff}$, the peak load P^* is less than debonding load P_{deb}.) Further increases in global slip result in a decrease in applied load until the fibers are completely debonded from the matrix, where the only residual contribution to the applied load is provided by interlocking. Thus, the load response becomes constant (point D) with an applied load value P_f associated with interlocking between single filaments and between fibers and matrix (see DS_330_60_D_3 in Fig. 9a). Fig. 10a also shows the stress-transfer mechanism stages corresponding to different states of the load response, where l_r is the residual bonded length, and other variables were defined previously.

It is worth noting that while the peak load P^* of single-lap shear tests can be measured directly, the value of P_{deb} for the PBO-FRCM composite is not easily determined from the load response because of the increase in applied load due to inter-locking as the STZ translates along the bonded region (region B−C of Fig. 10a). The authors previously used a fracture mechanics approach to determine the value of P_{deb} and the effective bond length l_{eff} from strain profiles along the bonded length [10,12]. The value of the applied load P_f can also be measured directly and used to determine the shear stress associated with interlocking, τ_f [10]:

$$\tau_f = \frac{P_f}{2nb^*\ell} \tag{13}$$

which in turn can be used to determine the difference in magnitude between P^* and P_{deb} if the effective bond length l_{eff} is known [10]:

$$P^* - P_{deb} = 2\tau_f nb^*\left(\ell - l_{eff}\right) \tag{14}$$

Based on experimental evidence from the double-lap shear tests discussed in Section 4.1, the idealized applied load-global slip response shown in Fig. 10a should characterize the $P_{II} - g$ response of the FRCM-concrete interface tested using the double-lap shear test (with P=P_{II}), although with several key differences related to the sequence of debonding in the two composite strips. With the double-lap shear test, debonding can occur in one of three possible scenarios illustrated in Fig. 10b: 1) debonding initiates in one composite strip, and debonding does not initiate in the other strip; 2) debonding initiates first in one composite strip, and then debonding initiates in the other composite strip; or 3) both of the composite strips debond simultaneously. For the double-lap shear tests in this study, either Scenario 1 or 2 occurred in each specimen (e.g., see Fig. 3), however, additional measurements are needed in the future to distinguish among these two scenarios. The responses in Fig. 9 show that the initial branch of the load response of the double-lap shear tests should be similar to region O-A shown in Fig. 10a. For the case of $\ell > l_{eff}$ for all three scenarios, after debonding initiates in the first composite strip (or both strips simultaneously for Scenario 3) ($P_{II} = P_{deb}$, corresponding to point B in Fig. 10a), the STZ translates along the bonded length to the free ends of the composite. Accordingly, interlocking between single fiber filaments and between fibers and matrix [19,20] should occur in the portion of the composite strip where the fibers have debonded, and consequently an increase in the applied load P_{II} should be observed. Once the STZ reaches the free end of the composite, the maximum load $P_{II}{}^*$ is reached (corresponding to point C in Fig. 10a). For Scenarios 1 and 2, unsymmetrical debonding causes unequal global slip of the two composite strips, which eventually causes the specimen to rotate (see Fig. 7b). The rotation could also start before debonding due to differences in local bonding conditions causing considerably more global slip in one strip than the other. The rotation causes further differences in applied loads in the two composite strips, as well as force components that are out of plane of the composites (Fig. 6), resulting in mixed mode conditions [17]. Further increases in displacement of the specimen (i.e., average of the LVDTs) result in increases in global slip in the composite strip that initially debonded, and a corresponding decrease in applied load, until the fibers are completely debonded from the matrix. At this point, the residual contribution to the applied load is provided by both interlocking and friction (Fig. 6). Thus, the value of the applied load at this point should be larger than the value associated with interlocking only (i.e., $P_{II} > P_f$ at point D in Fig. 10a), as confirmed by the load responses shown in Fig. 9b. Accordingly, the value of the applied load at point D cannot be used to determine the debonding load using Eqs. (13) and (14).

For Scenario 3, simultaneous debonding in both composite strips theoretically should maintain the symmetry of the system, and no rotation should occur. Accordingly, the applied load and global slip in each composite strip should be equal throughout the entire test, and the entire idealized load response of both strips should be similar to that shown in Fig. 10a. While Scenario 3 is theoretically possible, it was not observed in the double-lap shear tests reported in this paper.

Unlike with the single-lap shear test, the peak load of the response of the double-lap shear test cannot be measured directly; however the assumption of perfect symmetry resulted in a reasonable approximation of P^*, as discussed in Section 4.1. The peak loads of the double-lap shear specimens (using the approximate value determined by Eq. (1)) and single-lap shear specimens are compared in Figs. 4 and 5 in terms of peak stress σ^*. Fig. 4 plots the relationship between σ^* and composite bonded length ℓ for specimens with a composite width b_1 equal to 60 mm (2.4 in.) for the DDS_XXX_60 series (double-lap shear specimens) and the DS_XXX_60 series (single-lap shear specimens), along with their respective average values plotted in the graph with solid markers. The average ultimate stress of the DDS_XXX_60 series is slightly lower than that of the DS_XXX_60 series for a given bonded length, with the exception of ℓ = 100 mm (3.9 in.). In general, the lower ultimate stress of the double-lap shear tests can be explained by the observation that debonding does not occur equally and simulta-neously in both composite strips (as was the case for all double-lap shear tests in this study). For the case of a single-lap shear test, the bond strength is the result of one bonded composite, whereas the bond strength determined from a double-lap shear test is the lesser result of two bonded composites (with two bonded surfaces for each strip). Another consequence of this difference is that, in gen-eral, single-lap shear tests should have more variability (scatter) than double-lap shear tests. Results in Fig. 4 support this hypothesis since the results of the double-lap shear test have less scatter than those of the single-lap shear tests, although it should be noted that fewer double-lap shear tests were conducted than single-lap shear tests. For the case of ℓ = 100 mm (3.9 in.), the ultimate stress of the single-lap shear tests is lower than that of the double-lap shear tests. This may be due to the influence of a fracture mechanics Mode-I effect that influences the results of the single-lap shear tests, especially those with relatively short composite bonded

lengths [17,21,22].

Fig. 4 also shows that the trends exhibited by both the DDS_XXX_60 and DS_XXX_60 series are similar. From the results of single-lap shear tests, the authors found that the $\sigma^* - \ell$ relation alone cannot be used to determine the effective bond length because of the contribution from interlocking for $\ell > l_{eff}$. Instead, strain profiles along the bonded length of single-lap shear test specimens were analyzed to investigate the stress-transfer mechanism at the matrix–fiber interface and determine the effective bond length, which was determined to be approximately 260 mm (10.2 in.) for the PBO-FRCM composite studied [10]. Results of the double-lap shear tests presented in Fig. 4 are in good agreement with these findings.

Fig. 5 shows the relation between peak stress σ^* and composite bonded width b_1 for specimens with the same bonded length (ℓ = 330 mm [13 in.]) for the DDS_330 series (double-lap specimens) and the DS_300 series (single-lap specimens). Average values of σ^* for each series and the same bonded width are plotted in the graph with solid markers. Also, the average values of σ^* for all specimens in the DDS_330 series and the DS_330 series are reported in the figure. The average value of the DDS_330 series is 6.5% lower than that of the DS_330 series (if $\sigma_{II}{}^*$ is considered instead, the average value of the DDS_330 series is 7.4% lower than the average value of the DS_330 series). Results from both the double-lap and single-lap shear tests are consistent and show that a width effect does not exist for this type of composite.

4.3. Summary

In summary, the results in Sections 4.1 and 4.2 show that debonding of the PBO-FRCM composite–concrete interface can be inferred from both the single-lap and double-lap shear tests. An advantage to the single-lap shear test is its simplicity; because force is applied directly to the composite, the force in the composite can be measured directly rather than determined indirectly from a local strain measurement or from measured displace-ments. However, the eccentricity of the applied load with respect to the support restraint cannot be fully eliminated, and a Mode-I condition may prevail for specimens with short composite bonded lengths [22]. Double-lap shear tests utilize a symmetrical system to apply load simultaneously to two bonded composite strips. The assumption of perfect symmetry appears to be reasonable in determining the peak load in the composite from the peak force applied to the test specimen. However, a procedure similar to the one presented in this paper must be used to determine the entire load-global slip response. Unlike the single-lap shear test, the value of the applied load at the end of the load response (point D in Fig. 10a) includes friction, and therefore it cannot be used to determine the shear stress associated with interlocking τ_f or the debonding load P_{deb} (Eqs. (13) and (14)). Finally, the peak loads measured using double-lap shear tests were found to be slightly lower than those of corresponding single-lap shear tests. In double-lap shear tests, debonding generally does not occur equally and simultaneously in both composite strips, and thus one of the composite strips debonds before the other strip. The composite strip that debonds first is expected to have the lower bond capacity of the two strips. In general, this would suggest that results from double-lap shear tests tend towards a lower bound estimate of the composite bond strength, as shown in this study. For these reasons, the authors recommend that the single-lap shear test be the preferred test setup to study the behavior of the FRCM-concrete joint.

5. Conclusions

This paper describes the results of an experimental study conducted to investigate the behavior and stress-transfer mechanism of PBO-FRCM composites externally bonded to a concrete substrate. Double-lap (direct) shear tests were conducted on specimens with composite strips bonded to concrete blocks. Parameters varied were composite bonded length and bonded width. Results were compared to those of single-lap shear tests of the same composite to examine the influence of test setup on the results. The following conclusions are made based on the findings of this study:

1. For each of the double-lap shear test specimens a single composite strip debonded, where debonding was characterized by slippage between the fibers and matrix within the composite strip. No damage was observed to the concrete prisms.
2. For each of the double-lap shear test specimens, different load responses were observed for the two FRCM composite strips, especially after the peak force was reached. The applied load - global slip response of the bonded composite reported for a given double-lap shear test specimen should be that of the composite strip that initially debonded. A procedure was developed and presented to determine the load response of the composite strip that debonded.
3. For double-lap shear test specimens, the simplified procedure assuming perfect symmetry is reasonable in determining the peak load in the bonded composites; however it is not valid to describe the post-peak response of the bonded composite (especially the global slip) unless simultaneous debonding occurs and perfect symmetry is maintained.
4. The idealized load responses of single-lap and double-lap shear tests are similar until the peak load is reached. If debonding occurs simultaneously in both composite strips, the entire load response should be similar. If debonding occurs in one composite strip before the other, the value of the constant load at the end of the test should be larger than that of the single-lap test because of friction due to the out-of-plane force component in the composite strip in addition to interlocking between the fibers or between the fibers and the matrix.
5. Certain aspects of the behavior of the FRCM-concrete interface that can be determined using the single-lap shear test, such as interlocking between single filaments and between fibers and matrix, cannot be determined using the double-lap shear test unless perfect symmetry is achieved and maintained throughout the entire test.
6. The ultimate stress of the double-lap shear test specimens was slightly lower than that of the single-lap shear tests for specimens with the same composite bonded length and bonded width. Differences in local bonding conditions due to stochastically distributed local variations of the bond characteristics are more pronounced with double-lap shear tests because double-lap shear tests have a larger number of bonded regions than single-lap shear tests, and the lowest bond strength governs the behavior. Less scatter in the ultimate load was observed in results of double-lap shear test results than those of single-lap shear tests.
7. A width effect was not observed with specimens tested using double-lap shear tests. These findings are consistent with results of single-lap shear tests of the same composite.

Acknowledgments

The experimental work discussed in this paper was conducted at Missouri University of Science and Technology (Missouri S&T). The authors would like to express their appreciation to the National

University Transportation Center (NUTC) at Missouri S&T for providing financial support for this project. Ruredil S.p.A. of San Donato Milanese, Italy, is gratefully acknowledged for providing the composite materials.

References

[1] L. De Lorenzis, G. Zavarise, Modeling of mixed-mode debonding in the peel test applied to superficial reinforcements, Int. J. Solids Struct. 45 (20) (2008) 5419–5436.
[2] C. Czaderski, K. Soudki, M. Motavalli, Front and side view image correlation measurements on FRP to concrete pull-off bond tests, J. Compos. Constr. 14 (4) (2010) 451–463.
[3] E. Martinelli, C. Czaderski, M. Motavalli, Modeling in-plane and out-of-plane displacement fields in pull-off tests on FRP strips, Eng. Struct. 33 (12)(2011) 3715–3725.
[4] A. Bilotta, F. Ceroni, E. Nigro, M. Di Ludovico, M. Pecce, G. Manfredi, Bond efficiency of EBR and NSM FRP systems for strengthening of concrete members, J Compos. Constr. 15 (5) (2011) 757–772.
[5] M.R. Valluzzi, D.V. Oliveira, A. Caratelli, G. Castori, M. Corradi, G. de Felice, E. Garbin, D. Garcia, L. Garmendia, E. Grande, U. Ianniruberto, A. Kwiecień, M. Leone, G.P. Lignola, P.B. Lourenço, M. Malena, F. Micelli, M. Panizza, C.G. Papanicolaou, A. Prota, E. Sacco, T.C. Triantafillou, A. Viskovic, B. Zając, G. Zuccarino, Round robin test for composite to brick shear bond characterization, Mater. Struct. 45 (12) (2012) 1761–1791.
[6] C. Pellegrino, D. Tinazzi, C. Modena, Experimental study on bond behavior between concrete and FRP reinforcement, J Compos. Constr. 12 (2) (2008) 180–189.
[7] H. Toutanji, Y. Deng, Comparison between organic and inorganic matrices for RC beams strengthened with carbon fiber sheets, J. Compos. Constr. 11 (5) (2007) 507–513.
[8] A. Nanni, A new tool for concrete and masonry repair – strengthening with fiber-reinforced cementitious matrix composites, Concr. Inter. 34 (2012) 43–49.
[9] T. D'Antino, L.H. Sneed, C. Carloni, C. Pellegrino, Bond behavior of the FRCM-concrete interface, in: Proceedings of the 11th International Symposium on Fiber Reinforced Polymer Reinforcement for Concrete Structures, FRPRCS-11, Guimaraes, Portugal, 2013.
[10] T. D'Antino, C. Carloni, L.H. Sneed, C. Pellegrino, Matrix-fiber bond behavior in PBO FRCM composites: a fracture mechanics approach, Eng. Fract. Mech. 117 (2014) 94–111.
[11] L.H. Sneed, T. D'Antino, C. Carloni, Investigation of bond behavior of PBO fiber-reinforced cementitious matrix composite-concrete interface, ACI Mater. J. 111 (5) (2014) 569–580.
[12] C. Carloni, T. D'Antino, L.H. Sneed, C. Pellegrino, The role of the matrix layers in the stress-transfer mechanism of FRCM composites bonded to a concrete substrate, J Eng. Mech. 141 (6) (2014), http://dx.doi.org/10.1061/(ASCE)EM.1943-7889.0000883.
[13] A. D'Ambrisi, L. Feo, F. Focacci, Bond-slip relations for PBO-FRCM materials externally bonded to concrete, Compos. – Part B Eng. 43 (8) (2012) 2938–2949.
[14] A. D'Ambrisi, L. Feo, F. Focacci, Experimental analysis on bond between PBO-FRCM strengthening materials and concrete, Compos – Part B Eng. 44 (1) (2013) 524–532.
[15] X. Ruredil, Mesh Gold Data Sheet, Ruredil S.p.A, Milan, Italy, 2009.
[16] K.V. Subramaniam, C. Carloni, L. Nobile, An understanding of the width effect in FRP-concrete debonding, Strain 47 (2) (2011) 127–137.
[17] P. Carrara, D. Ferretti, A finite-difference model with mixed interface laws for shear tests of FRP plates bonded to concrete, Compos – Part B Eng. 54 (2013) 329–342.
[18] C. Carloni, K.V. Subramaniam, Application of fracture mechanics to debonding of FRP from RC members, in: A Fracture Approach for FRP-Concrete Structures, SP-286, ACI, 2012.
[19] B. Banholzer, Bond Behavior of Multi-filament Yarn Embedded in a Cementitious Matrix (Ph.D. thesis), RETH Aachen University, Aachen, Germany, 2004.
[20] J. Hartig, U. Häußler-Combe, K. Schicktanz, Influence of bond properties on the tensile behaviour of textile reinforced concrete, Cem. Concr. Compos. 30 (2008) 898–906.
[21] P. Carrara, D. Ferretti, F. Freddi, G. Rosati, Shear tests of carbon fiber plates bonded to concrete with control of snap-back, Eng. Fract. Mech. 79 (2011) 2663–2678.
[22] J. Yao, J.G. Teng, J.F. Chen, Experimental study on FRP-to-concrete bonded joints, Compos – Part B Eng. 36 (2005) 99–113.